

Liquid Metal pH Morphology Sensor Used for Biological Microenvironment Detection

Yang Wang, Liangtao Li, Shuting Liang, Kang Sun, Caicai Jiao, Qian Wang, and Liang Hu*



Cite This: <https://doi.org/10.1021/acs.analchem.2c04357>



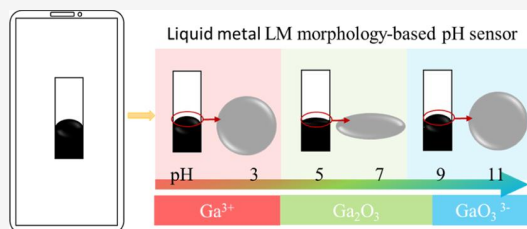
Read Online

ACCESS |

Metrics & More

Article Recommendations

ABSTRACT: pH is one of the important parameters of a biological microenvironment, which is closely related to cell growth, development, vitality, division, and differentiation. Monitoring the pH of a microenvironment is helpful to monitor the cell metabolism as well as to understand the cellular life cycle. The sensitivity of liquid metals (LMs) to hydrogen ions has aroused our interest. Here, we propose a novel but facile pH sensor using liquid gallium (LM for short) droplet morphological change as the readout. The pH sensing characteristics of the LM droplet were examined, especially the shape response. LM can form solid native oxide skin rapidly in oxygenated solution, and the oxide layer will be removed in acidic or alkaline solutions, which will cause a great change in surface tension. The phenomenon is the change of LM morphology from macroscopic observation. We explored the electrochemical characteristics of LM at different pH values, explained the mechanism of surface change, and calibrated the relationship curve between LM morphology and pH and the interference of impurity ions on the sensor. Finally, we proposed a detection algorithm for the LM pH morphology sensor and tried to automatically detect pH with a mobile app, which was applied to the pH detection of cell culture solution. We believe that the response characteristics of LM to hydrogen ions have great potential in microenvironment detection.



INTRODUCTION

Studying cell growth, development patterns, and functions *in vitro* by culturing cells in a simulated *vivo* environment is an important tool in modern life sciences, and pH detection is of great value in the cellular microenvironment.^{1,2} Hydrogen ion, which directly reflects the pH of the cellular microenvironment, plays an important role in cell growth, development, and division.^{3,4} In general, the pH of the cellular environment is dynamically balanced within a range of 7–9, while the pH of cancer cells can reach 5.5.⁵ Various methods have been developed to detect pH, ranging from traditional pH sensors to new pH detection devices⁶ including optical sensors,⁷ electrochemical sensors,⁸ visual sensors,⁹ and so forth. Common commercial pH sensors rely on the electrochemical principle to detect the potential of the solution, which is dependent on the hydrogen ion concentration of the solution.¹⁰ These pH test devices are complicated to operate and require tedious titration and maintenance. The test results are susceptible to the interference of ions in the solution.¹¹ Traditional measurement methods are not suitable for complex biological systems.

Therefore, new pH detection devices have been invented in recent years with convenient and simple features to adapt to complex biological microenvironments.¹² Li et al. studied a pH sensor for wound healing using microelectronic processing technology combined with the capability of a pH-sensitive polyaniline membrane,¹³ which can detect the pH of skin

wounds in real time. Li et al. developed a visual pH sensor using polyvinyl alcohol and dye-modified cellulose for food spoilage detection.¹⁴ Tang et al. prepared a refractive index pH-sensitive polymer optical sensor for pH detection of serum.¹⁵ New pH test devices tend to be costly and complicated to prepare, which can bring significant cost increases when batch-scale pH detection is required. Novel low-cost, simple-to-operate, and responsive pH sensors for biological microenvironments need to be developed.¹⁶

The room temperature liquid metals (LMs) represented by Gallium and gallium-based alloys have attracted much attention in recent years. Attributed to their special fluidity, electrical conductivity, and deformability, they are widely used in flexible electronics,¹⁷ microfluidics,¹⁸ sensors,¹⁹ and actuators.²⁰ The pH-responsive properties of LMs have been reported in the past few years, including the special electric double layer (EDL) structure of LMs under acidic and alkaline conditions,²¹ the large deformation and motion caused by the sudden change of surface tension, Marangoni flow of LMs

Received: October 4, 2022

Accepted: November 23, 2022

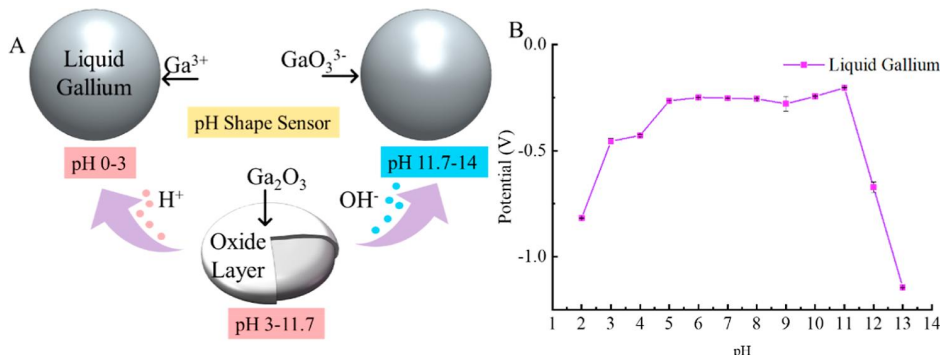


Figure 1. LM (A) surface reaction and (B) potential in different pH.

caused by different pH,²² the van der Waals force traction motion of LMs,²³ and so on. On the other hand, LMs have certain biosafety and have been applied in the research of electronic artificial blood vessels,²⁴ nerve electrodes,²⁵ contrast agents,²⁶ drug-loaded microspheres,²⁷ and so on. Based on the abovementioned characteristics, we found the possibility of using LM to prepare a pH sensor and made an attempt in this research.

In this study, we proposed a novel pH sensor based on LM morphological change and applied it to the detection of pH in the cellular microenvironment. We used LM to display the shape characteristics of different pH, calibrated the morphology-pH response, and tried to explain the morphology change from the theory of electrochemistry and surface tension. A low-cost and easy-to-use pH sensor was studied and used to determine the pH of the cell culture medium. Finally, we used a mobile phone app for LM morphology recognition to detect pH, which may be used for batch automatic detection of cell microenvironment in the future.

MATERIALS AND METHODS

Preparation of the Liquid Gallium Electrode and pH Potential Measurement. The melted pure gallium (99.99%) was filled into a silicone rubber hose with the 2 mm inner diameter by a disposable syringe, and a copper foil with 1 mm width was placed into it as the electrode connecting line. The LM rubber and copper foil were put into a refrigerator at -18°C for 24 h to freeze into a fixed electrode shape. The infiltration force between the copper and LM can guarantee good fixation and connection.²⁸ Then, the electrode was taken out and partially heated, and the lower gallium was melted in the silicone tube. 2–13 pH solutions were prepared by quantitative mixing of 0.1 mol·L⁻¹ HCl and NaOH, and then, the pH meter was used for calibration. The prepared electrode was used as the working electrode and the platinum electrode as the auxiliary electrode, and the reference electrode was selected according to acidity and alkalinity (Hg/Hg₂Cl₂ electrode used in acidic, Ag/AgCl electrode used in neutral, Hg/HgO electrode used in alkaline solution) and connected to the electrochemical workstation (CHI660E Huachen Shanghai). The open circuit voltage was measured to get the potential of LM at different pH.

Cyclic Voltammetry Test of the LM Electrode. The cyclic voltammetry test was carried out in the three-electrode system, with the homemade LM electrode as the working electrode, the reference electrode changed according to the acidity and alkalinity of the solution, and the platinum disk electrode as the auxiliary electrode. The cyclic voltammetry

parameters were set in the voltage range of -0.2 to -1.8 V, the working mode was negative, and the scanning speed was 0.1 V/s. The cyclic test voltage range was determined by the open circuit voltage.

LM Electrode Potential and Ion Interference under Different pH by Chronoamperometry. The response of the liquid gallium electrode to different ions at an applied voltage of -0.8 V with a stable current was studied by the chrono-current method. Different pH solutions were replaced in the electrochemical reaction cell, and the time current change curve was recorded. The current reached a relatively stable value after 150 s, and so, the current value of 175–200 s was selected as the study object. After that, the interference of different ions was explored in the pH 7 environment by adding 100–400 μL of impurity ions in 2 mL of 0.1 mol·L⁻¹ NaCl solution (all impurity ion concentrations were 0.1 mol·L⁻¹).

Effect of pH and Impurity Ions on the Morphology of LM. The different pH solutions were added into a square tube with the size of $3 \times 8 \times 15$ mm, and 200 μL of LM was injected slowly. The square tube was fixed in front of the high-speed camera to obtain the morphology of the LM in different pH solutions. The distance between the camera lens and the square tube was between 20 and 23 cm. In the impurity ion experiment, different types and different volumes of impurity ion solution were added into the 200 mL of prepared pH solution, and then, 200 μL LM was injected.

Image Acquisition and Feature Extraction of Morphological Photographs. The mobile phone was placed 20–23 cm in front of the square tube and a picture with a resolution greater than 800×400 was photographed by the mobile phone. The image was binarized, and the coordinates of the morphology of LM were extracted from the image. The leftmost and rightmost ends of the arc plane were set as X_1 , X_2 , and the top and bottom as Y_1 , Y_2 . The radian prominence was defined as k , $k = H/X = |Y_1 - Y_2|/|X_1 - X_2|$.

Biological Microenvironment pH Assay. The culture solution of mouse osteoblasts cultured for 3 days was taken and the pH was adjusted with 0.1 mol·L⁻¹ HCl and NaOH to form a pH 5–8 culture solution. After that, 200 mL of the solution was added to the square tube and 200 μL of LM was slowly added for morphological observation.

RESULTS AND DISCUSSION

Principle of the LM pH Sensor. In a solution dissolved with oxygen, such as water, ethanol, and so forth, a thin oxide layer is easily formed on the surface of LMs.²⁸ The oxide layer with a thickness of 1–3 nm is similar to the skin of LMs in appearance, the self-limiting oxide layer protects the metal

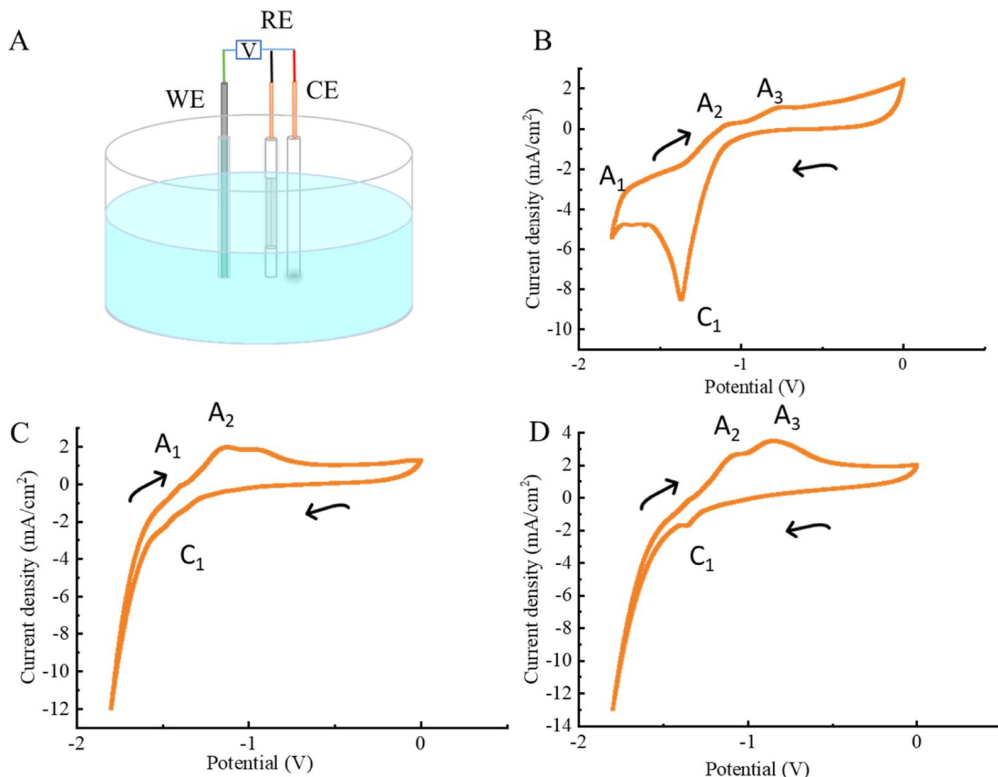


Figure 2. (A) Schematic diagram of the electrochemical test. (B–D) LM cyclic voltammetry results in pH 2, 7, and 12 solutions.

from further oxidation, and thickening of the surface oxide occurs only slowly, which protects the internal LMs from further oxidation.²⁹ At the same time, the formation of the oxide film will greatly reduce the surface tension of LMs.³⁰ In previous studies, scholars controlled the generation and removal of the oxide layer by applying voltage or adjusting the pH in the solution environment, which enabled the LMs to deform and move.³¹ We found that the oxide layer state of LMs in different pH values is different. In strong acidic or alkaline solutions, the oxide layer of LMs can be completely removed, while it will exist in the solution with a pH between 2 and 12.²² The main composition of the oxide layer is Ga₂O₃, which is also called passive film.³⁰ When the gallium-based liquid alloy is placed in the alkaline solution, the charge accumulation at the interface of the negatively charged LM leads to the attraction of the opposite layer containing positively charged ions in the electrolyte.³² In acidic solution, the formation of Ga³⁺ was observed and the polarity of EDL was reversed.³² As shown in Figure 1A, when LM is in a strongly acidic environment, the oxide layer is removed, and the LM curls into a sphere. When the solution environment becomes neutral, the oxide layer of the LM thickens, the surface tension decreases, and the LM collapses into a flat shape. When the solution becomes alkaline, the oxide layer is removed again. At this time, the surface ion of the LM is GaO₃³⁻, the surface tension increases, and it curls into a sphere. This characteristic inspired us to invent the LM pH morphology sensor. Interestingly, the digestion of LM in solution is almost negligible, and a 3 mm diameter LM droplet micropump can theoretically operate for 42 days in the alkaline environment.³³ Particularly, the LM droplet was only in contact with the solution for a short time, and then, it would be recycled in alkali solution.³⁴ Since the eutectic bond of LM is

very stable, the stability of the interface ensures that the internal LM will not be contaminated.³⁵

Electrochemical Mechanism and Process Analysis. To describe the change of surface tension, we tested the potential of the LM electrode in different pH solutions with an electrochemical workstation. As shown in Figure 1B, the potential of the LM gradually increased from −0.8 to −0.25 V when the pH was changed from 2 to 7. When the pH was close to neutral, the potential was kept at a stable value. When the pH continued to increase, the surface potential of the LM dropped suddenly and finally dropped to −1.1 V at pH 13. The potential of the LM electrode showed that the oxide layer on the surface of LM reacts with hydrogen ions, and it has an obvious response to the concentration of hydrogen ions. This directly affected the surface tension of the LM. The LM and the solution formed an EDL structure. According to Lippmann's equation, $\gamma = \gamma_0 - \frac{1}{2}CU^2$, γ is the surface tension of the LM, γ_0 is the value of maximum surface tension, C is the capacity per unit area of the EDL, and U is the surface potential difference of LMs.³⁰ The result of surface tension and the potential in solution is consistent with the chemical reaction on the surface of the LM.

Reactions on the Surface of the LM at Different pH Values. Taking pH 2, 7, and 12 as the typical reaction, a cylindrical self-made gallium electrode was used as the working electrode, as shown in Figure 2A. Cyclic voltammetry of the electrochemical workstation was used to explore the surface reaction. Figure 2B–D shows the cyclic voltammetry curve of the gallium electrode in the solution with pH of 2, 7, and 12. We speculated that the C₁ peak was the peak in which gallium was used as the cathode in water and reacts with H⁺, and the reaction formula is $2H^+ + 2e^- \rightarrow H_2$. A₁ represented the polarization process of the gallium electrode, A₂ was the

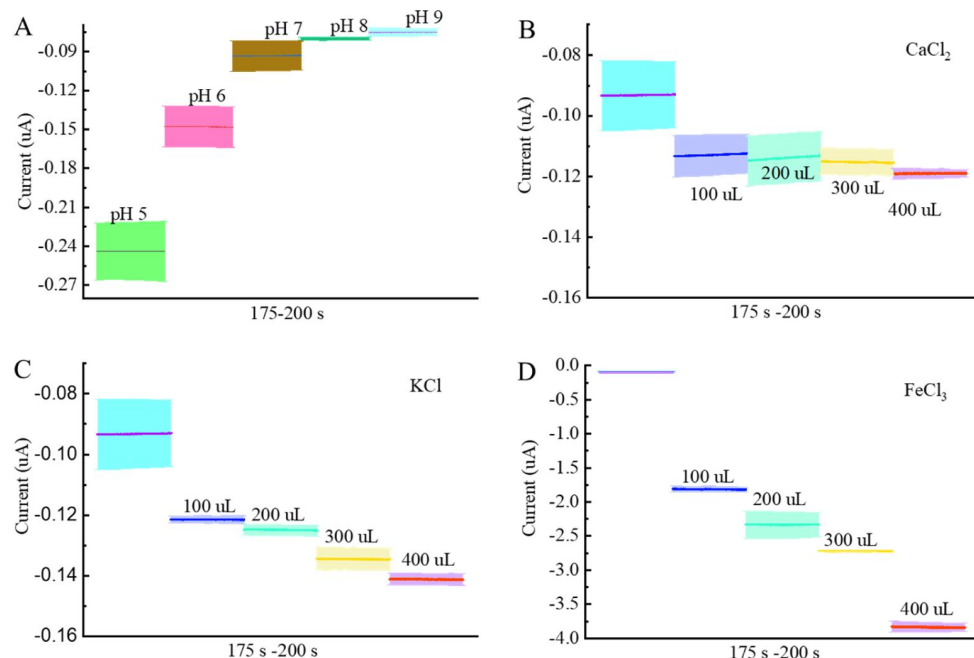


Figure 3. (A) LM stable current at -0.8 V voltage in different pH solutions. The impact of different doses (B) CaCl_2 , (C) KCl , and (D) FeCl_3 on LM current in pH 7 solution.

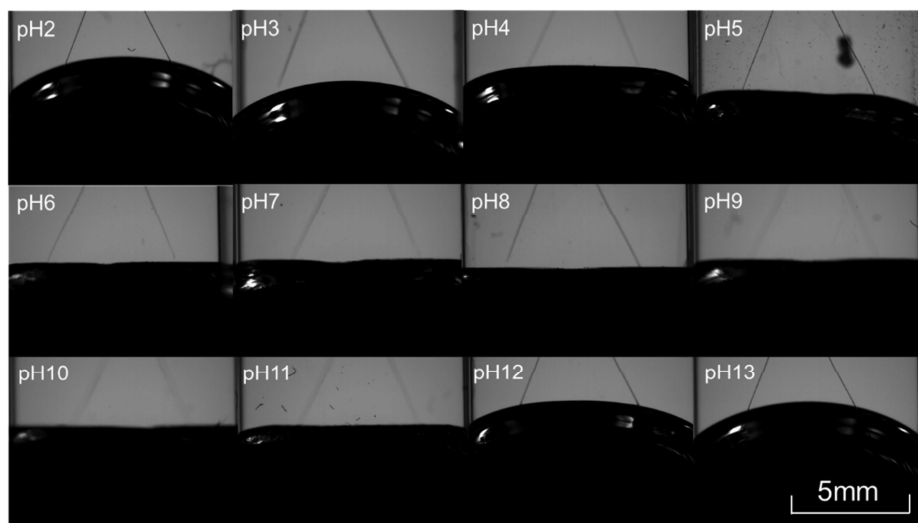


Figure 4. Surface morphology photographs of LM in different pH solutions.

process of the electrode forming an EDL, and the A_3 peak was that Ga is oxidized to Ga^{3+} with the reaction formula $\text{Ga} - 3\text{e}^- \rightarrow \text{Ga}^{3+}$.³⁶ In Figure 2B, it could be observed that with the application of reduction potential, reduction of hydrogen ions occurred on the surface of the gallium electrode at -1.4 V potential. While the pH of the solution was 7, there was only C_1 peak, indicating that H^+ was reduced on the gallium electrode, but the C_1 peak was not obvious.³⁷ We speculated that it was caused by the reduction of hydrogen ion concentration.³⁸ A_1 and A_2 were the processes of electrode polarization and EDL formation. In Figure 2C, the peak of A_1 moved obviously to the right and the peak was unsharp, and the A_3 peak was not observed in this curve, which indicated that the oxide layer on the surface of LM had been formed at pH 7 and could not continue to produce under an oxidation potential. Figure 2D shows the cyclic voltammetry curve of the

LM electrode at pH 12. The reduction peak C_1 in the figure was similar to the previous one, but there was no peak A_1 . The gallium electrode produced an EDL structure, and then, Ga produced Ga^{3+} at the oxidation potential.³⁹ According to the cyclic voltammetry curves of LM electrodes at different pH values, it could be verified that the interface reaction on the surface of LM was highly correlated with hydrogen ion concentration, and it also verified our conjecture that the interface morphology of the LM was sensitive to hydrogen ion concentration, which was our theoretical basis for designing the morphological response of LM.

Attempt to Measure pH Electrochemically with the Gallium Electrode. We measured the influence of different pH on the current of the LM electrode and studied the response of stable current of the LM electrode to pH when applied with -0.8 V voltage by chronoamperometry. In the

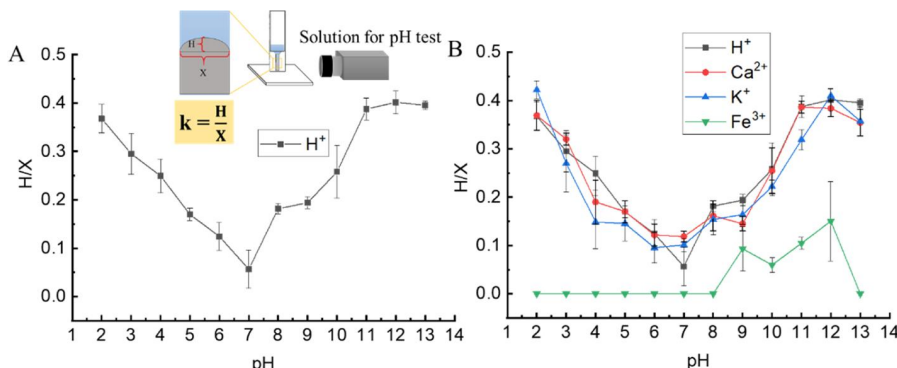


Figure 5. (A) Ratio of LM convex surface diameter to height in different pH solutions. (Illustration: schematic diagram for calculating the convex liquid surface.) (B) Ratio of LM convex surface diameter to height under the interference of different ions.

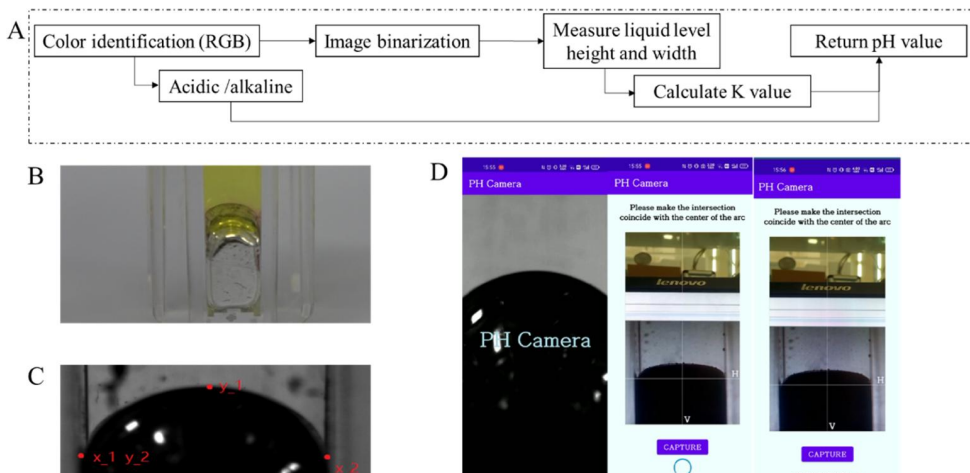


Figure 6. Automated pH detection. (A) Flow chart of the automatic pH detection algorithm. (B) Photograph of the solution waiting to be tested and the LGM sensor. (C) Black and white image after image processing. (D) Screenshot of a video of the phone software detecting pH.

timing current method, the current value decreased rapidly and then reached a nearly stable state. The experimental results were stable after 150 s. The experimental results are shown in Figure 3A. With the increase of pH, the surface current of LM decreased, which indicated that the concentration of H^+ can be electrochemically detected by the gallium electrode. However, considering the complexity of the solution detection environment, we verified the interference of Ca^{2+} , K^+ , and Fe^{3+} on electrochemical detection under the condition of pH 7, as shown in Figure 3B–D. With the addition of impurity ions, the current increased and changed obviously, proving that the electrochemical measurement of pH by the gallium electrode was easily interfered by impurity ions. If the gallium electrode is considered as a pH electrochemical sensor, the electrode needs to be packaged. The interference of pre-impurity ions can be prevented by the glass film or selective ion permeable film, but the preparation cost is high. What is worse, electrochemical measurement relies on the filter and amplifier to deal with the potential signal, and the device depends on complex circuits. By contrast, a simpler strategy is to use the response of LM morphology to hydrogen ions.

Morphology Characteristics of LM at Different pH Values. A group of LM photographs in Figure 4 showed the corresponding morphology at different pH. When the pH was 2–3, the surface showed obvious metallic luster in the vessel. When the pH was 4 and 5, the convex liquid level became

inconspicuous, and the surface luster got slightly darker. When the pH was 6–9, the LM droplet was basically a plane, and the surface luster was dimmer. However, with the increase of pH, the droplets gradually became more convex from pH 10, and the liquid surface gradually brightened. The LM oxide layer is thinner in acid and alkali solutions and thicker in neutral environments.

Standard Curve of the pH Sensor Based on LM Morphology. A quantitative amount of LM was put into a square tube and observed the interface morphology between LM and solution with a high-speed camera (Figure 5A illustration). To describe this feature in detail, an aspect ratio is defined as k , $k = H/X$.

where H is the height of the LM convex surface and X is the restricted width of the LM. According to the research mentioned above, the LM surface will be more convex in strong acid or alkali solution, while in a nearly neutral solution, the LM surface will be flatter due to the decrease of surface tension.⁴⁰ According to the response of LM morphology to H^+ , we drew a standard detection curve, as shown in Figure 5A. The convexity was larger in acidic and alkali solutions. When the pH was 5–8, the LM was seriously oxidized in the solution and the liquid surface was flat. When the pH was larger than 8, the convexity increased with the pH. The oxide layer became thinner with the increase of pH in the alkali solution.

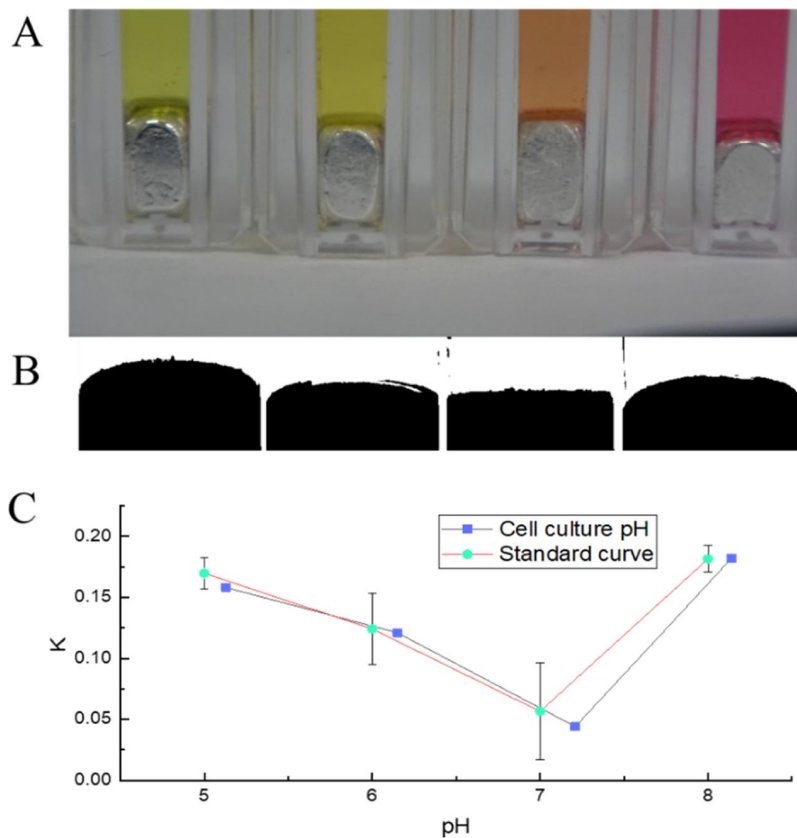


Figure 7. (A) Photographs of cell culture medium and LM. (B) LM morphology photographs after image processing. (C) pH and K value comparison between cell culture medium and standard curve.

According to the convexity curve, the LM is sensitive to H^+ and has good responsiveness.

Influence of Impurity Ions in Solution on the Sensor.

We verified the effects of Ca^{2+} , K^+ , and Fe^{3+} ions on the morphology of LM. As shown in Figure 5B, Ca^{2+} and K^+ had little influence on the calibration of the sensor, while Fe^{3+} ions affected the sensor severely. K^+ and Ca^{2+} did not participate in the reaction between Ga_2O_3 and H^+ ions, which had no influence on the morphology of LM. Therefore, the morphology sensor of LM can be applied to pH detection of complex ion solutions containing K^+ , Ca^{2+} , and so on. However, Fe^{3+} had the oxidizing property, and it could participate in the oxidation-reduction reaction of Ga. Fe^{3+} was reduced to Fe^{2+} , while the Ga atom loses its electrons and is oxidized to Ga^{3+} , so the surface tension decreases, resulting in the liquid level of the LM becoming flat and no longer protruding.⁴¹ In an acidic environment, Fe^{3+} reacted with LM, while in an alkali environment, Fe^{3+} and OH^- combined to form reddish-brown precipitate $\text{Fe}(\text{OH})_3$, which also disturbed the signal acquisition of the vision sensor. Therefore, the gallium pH sensor is not suitable for the detection of impurity ions such as Cu^{2+} and Fe^{3+} , which can react with Ga. We believe that the Ga-pH sensor may be applied to the detection of the cell microenvironment because the cell microenvironment contains impurity ions such as K^+ and Ga^{2+} but nearly no Fe^{3+} and Cu^{2+} plasma.^{42,43}

Automatic pH Detection. According to the morphological characteristics and response, we designed the most used smartphone App to automatically calculate the pH of the solution. We use the mobile phone camera to obtain

information such as LM morphology state, solution color, the ratio of liquid surface arc height to width, and so forth to complete the calculation of pH according to the pre-measured data and standard curve. The specific algorithm is shown in Figure 6A. First, according to the picture information obtained by the camera, the three-channel RGB (red, green, blue) value of the collected image was analyzed, as shown in Figure 6B. The acid solution is pale yellow, while the alkali solution is red. Because the change characteristics of morphology sensing were not obvious when the pH was close to neutral, we added pH indicator color to assist the judgment. The R channel value in the alkali solution will be larger than that of the acid solution after normalization. Second, the specific pH value can be calculated through the LM morphology. According to the response characteristics of LM and solutions, the surface characteristics of LM will be different when the pH of the solution is different. We binarize the image with a threshold, so that the LM is black (0) and the rest is white (1) shown in Figure 6C. Calculating the ratio of the height and width of LM had the same specificity as the radian. We kept the pH value results as integers, so that each pH value corresponded to a range of aspect ratio values. By measuring and calculating, the aspect ratio section corresponding to each pH value is obtained. Figure 6D shows a video screenshot of the mobile App identifying the pH of the solution. After identification by the mobile App, the pH of the unknown solution to be measured was 5. Compared with the traditional pH sensors, the cheap LM morphology sensor is more convenient to use, and it is not limited by the power supply. Compared with the disposable pH test paper, the LM can be recycled and bring

environmental resource-saving benefits. The detection method through photo features is simpler and more programmed, which can be designed for automatically detecting in batches, reducing labor costs. The main cost of the LM pH morphology sensor is LM itself. According to the existing studies, the digestion of LM in acid and aqueous solution is relatively slow,³³ and more LM can be recycled, so the cost is lower than other pH sensors.

Biological Microenvironment Detection. To verify the performance of the LM pH sensor in detecting the pH of the cell microenvironment, we took the culture solution of mouse osteoblasts, which was adjusted to pH 5.13, 6.15, 7.21, and 8.14 by HCl and NaOH. As shown in Figure 7A, the morphology of LM in the solution with pH 5.13–8.14 is shown from left to right. After processing the images, obvious feature differences can be observed in appearance, as shown in Figure 7B, and the calculated values of k were 0.158, 0.121, 0.044, and 0.182 and the pH values obtained by substituting them into the standard curve are 5, 6, 7, and 8. The pH obtained by calculation was compared with the standard curve, as shown in Figure 7C, showing a good coincidence degree.

Although different pH values already show different colors by the acid–base indicator, accurate color recognition may be limited by light and subjective factors when reading. Combined with the morphology of LM to determine the pH, the identification results will be more accurate.

CONCLUSIONS

In this paper, we present a LM morphology-based pH sensor with simple operation and low cost. We explored the working mechanism of LM sensitive to hydrogen ions, calibrated the relationship between pH and morphology parameters, and learned the effect of different impurity ions on its measurement result. The morphology pH sensor was not affected by Ca^{2+} , Cl^- , and K^+ ions. Finally, we designed an App to automatically detect pH and verified its feasibility to detect cell culture fluid. In the future, we will improve this sensor system to make it suitable for more complex biological microenvironments.

AUTHOR INFORMATION

Corresponding Author

Liang Hu — Beijing Advanced Innovation Center for Biomedical Engineering, School of Biological Science and Medical Engineering, Beihang University, Beijing 100191, China;  orcid.org/0000-0003-1648-7696; Email: cnhliang@buaa.edu.cn

Authors

Yang Wang — Beijing Advanced Innovation Center for Biomedical Engineering, School of Biological Science and Medical Engineering, Beihang University, Beijing 100191, China

Liangtao Li — Beijing Advanced Innovation Center for Biomedical Engineering, School of Biological Science and Medical Engineering, Beihang University, Beijing 100191, China

Shuting Liang — Beijing Advanced Innovation Center for Biomedical Engineering, School of Biological Science and Medical Engineering, Beihang University, Beijing 100191, China

Kang Sun — Beijing Advanced Innovation Center for Biomedical Engineering, School of Biological Science and

Medical Engineering, Beihang University, Beijing 100191, China

Caicai Jiao — Beijing Advanced Innovation Center for Biomedical Engineering, School of Biological Science and Medical Engineering, Beihang University, Beijing 100191, China

Qian Wang — Beijing Advanced Innovation Center for Biomedical Engineering, School of Biological Science and Medical Engineering, Beihang University, Beijing 100191, China

Complete contact information is available at:
<https://pubs.acs.org/10.1021/acs.analchem.2c04357>

Author Contributions

The manuscript was written through contributions of all authors. All authors have given approval to the final version of the manuscript.

Notes

The authors declare no competing financial interest.

ACKNOWLEDGMENTS

This work is supported by National Natural Science Foundation of China (grant no. 81801794) and Beijing Municipal Natural Science Foundation China (grand no. 7202104 and grand no. L223017).

REFERENCES

- (1) Miranda Mugica, M.; McGuinness, K. L.; Lawrence, N. S. *Sensors* **2022**, *22*, 555.
- (2) Dabaghi, M.; Saraei, N.; Xu, G.; Chandiramohan, A.; Yeung, J.; Nguyen, J. P.; Vukmirovic, M.; Selvaganapathy, P. R.; Hirota, J. A. *Sci. Rep.* **2021**, *11*, 3477.
- (3) He, X.; Ding, F.; Sun, X.; Zheng, Y.; Xu, W.; Ye, L.; Chen, H.; Shen, J. *Sens. Actuators, B* **2021**, *332*, 129496.
- (4) Ocaña, C.; Brosel-Oliu, S.; Abramova, N.; Bratov, A. *Instrum. Sci. Technol.* **2021**, *49*, 288–303.
- (5) Karaçam, S.; Tunçer, S. *Probiotics Antimicrob. Proteins* **2022**, *14*, 995–1011.
- (6) Richter, A.; Paschew, G.; Klatt, S.; Lienig, J.; Arndt, K. F.; Adler, H. P. *Sensors* **2008**, *8*, 561–581.
- (7) Wang, S.; Zhang, Z.; Huang, Z.; Lei, X.; Wang, Y.; Li, L.; Yang, L.; Liu, H.; Sun, F.; Ma, L.-J. *J. Photochem. Photobiol., A* **2021**, *418*, 113438.
- (8) Manjakkal, L.; Dang, W.; Yogeswaran, N.; Dahiya, R. *Biosensors* **2019**, *9*, 14.
- (9) Ding, L.; Li, X.; Hu, L.; Zhang, Y.; Jiang, Y.; Mao, Z.; Xu, H.; Wang, B.; Feng, X.; Sui, X. *Carbohydr. Polym.* **2020**, *233*, 115859.
- (10) Richter, A.; Paschew, G.; Klatt, S.; Lienig, J.; Arndt, K.-F.; Adler, H.-J. P. *Sensors* **2008**, *8*, 561–581.
- (11) Jafari, B.; Muthuvell, M.; Botte, G. G. *J. Electroanal. Chem.* **2021**, *895*, 115547.
- (12) Liu, J.; Lu, W.; Zhang, L.; Yang, J.; Yao, Z.-P.; He, Y.; Li, Y. *Biosens. Bioelectron.* **2021**, *193*, 113534.
- (13) Li, Y.; Mao, Y.; Xiao, C.; Xu, X.; Li, X. *RSC Adv.* **2020**, *10*, 21–28.
- (14) Ding, L.; Li, X.; Hu, L.; Zhang, Y.; Jiang, Y.; Mao, Z.; Xu, H.; Wang, B.; Feng, X.; Sui, X. *Carbohydr. Polym.* **2020**, *233*, 115859.
- (15) Tang, Z.; Gomez, D.; He, C.; Korposh, S.; Morgan, S. P.; Correia, R.; Hayes-Gill, B.; Setchfield, K.; Liu, L. *J. Lightwave Technol.* **2021**, *39*, 1557–1564.
- (16) Chang, Y.; Wang, L.; Li, R.; Zhang, Z.; Wang, Q.; Yang, J.; Guo, C. F.; Pan, T. *Adv. Mater.* **2021**, *33*, 2003464.
- (17) Chen, X.; Wan, H.; Guo, R.; Wang, X.; Wang, Y.; Jiao, C.; Sun, K.; Hu, L. *Microsyst. Nanoeng.* **2022**, *8*, 48.
- (18) Yuan, B.; He, Z.; Fang, W.; Bao, X.; Liu, J. *Sci. Bull.* **2015**, *60*, 648–653.

- (19) Guo, R.; Wang, X.; Yu, W.; Tang, J.; Liu, J. *Sci. China: Technol. Sci.* **2018**, *61*, 1031–1037.
- (20) Sun, Y.; Xu, S.; Tan, S.; Liu, J. *Micromachines* **2018**, *9*, 192.
- (21) Khan, M. R.; Trlica, C.; Dickey, M. D. *Adv. Funct. Mater.* **2015**, *25*, 671–678.
- (22) Zavabeti, A.; Daeneke, T.; Chrimes, A. F.; O'Mullane, A. P.; Zhen Ou, J.; Mitchell, A.; Khoshmanesh, K.; Kalantar-zadeh, K. *Nat. Commun.* **2016**, *7*, 12402.
- (23) Guo, J.; Wang, Y.; Wang, X.; Xing, Y.; Hu, L. *Adv. Mater.* **2020**, *7*, 2070091.
- (24) Cheng, S.; Hang, C.; Ding, L.; Jia, L.; Tang, L.; Mou, L.; Qi, J.; Dong, R.; Zheng, W.; Zhang, Y.; Jiang, X. *Matter* **2020**, *3*, 1664–1684.
- (25) Tang, R.; Zhang, C.; Liu, B.; Jiang, C.; Wang, L.; Zhang, X.; Huang, Q.; Liu, J.; Li, L. *Biosens. Bioelectron.* **2022**, *216*, 114600.
- (26) Fan, L.; Duan, M.; Xie, Z.; Pan, K.; Wang, X.; Sun, X.; Wang, Q.; Rao, W.; Liu, J. *Small* **2020**, *16*, 1903421.
- (27) Lu, Y.; Lin, Y.; Chen, Z.; Hu, Q.; Liu, Y.; Yu, S.; Gao, W.; Dickey, M. D.; Gu, Z. *Nano Lett.* **2017**, *17*, 2138–2145.
- (28) Liu, S.; Qu, D.; McDonald, S.; Gu, Q.; Matsumura, S.; Nogita, K. *J. Alloys Compd.* **2020**, *826*, 154221.
- (29) Khan, M. R.; Trlica, C.; So, J. H.; Valeri, M.; Dickey, M. D. *ACS Appl. Mater. Interfaces* **2014**, *6*, 22467–22473.
- (30) Daeneke, T.; Khoshmanesh, K.; Mahmood, N.; de Castro, I. A.; Esrafilzadeh, D.; Barrow, S. J.; Dickey, M. D.; Kalantar-zadeh, K. *Chem. Soc. Rev.* **2018**, *47*, 4073–4111.
- (31) Zhao, X.; Xu, S.; Liu, J. *Front. Energy* **2017**, *11*, 535–567.
- (32) Yuan, B.; He, Z.-Z.; Liu, J. *J. Electron. Mater.* **2018**, *47*, 2782–2790.
- (33) Fu, J. H.; Liu, T. Y.; Cui, Y.; Liu, J. *Adv. Mater. Interfaces* **2021**, *8*, 2001936.
- (34) Ding, Y.; Zeng, M.; Fu, L. *Matter* **2020**, *3*, 1477–1506.
- (35) Tang, S. Y.; Khoshmanesh, K.; Sivan, V.; Petersen, P.; O'Mullane, A. P.; Abbott, D.; Mitchell, A.; Kalantar-zadeh, K. *Proc. Natl. Acad. Sci. U.S.A.* **2014**, *111*, 3304–3309.
- (36) Teng, L.; Ye, S.; Handschuh-Wang, S.; Zhou, X.; Gan, T.; Zhou, X. *Adv. Funct. Mater.* **2019**, *29*, 1808739.
- (37) Mao, Y.; Wu, Y.; Zhang, P.; Yu, Y.; He, Z.; Wang, Q. *Mater. Sci. Technol.* **2021**, *61*, 132–137.
- (38) Frumkin, A.; Polianovskaya, N.; Grigoryev, N.; Bagotskaya, I. *Electrochim. Acta* **1965**, *10*, 793–802.
- (39) Chung, Y.; Lee, C.-W. *J. Electrochem. Sci. Technol.* **2013**, *4*, 1–18.
- (40) Pandey, B.; Cox, C. B.; Thapa, P. S.; Ito, T. *Electrochim. Acta* **2014**, *142*, 378–385.
- (41) Mayyas, M.; Mousavi, M.; Ghasemian, M. B.; Abbasi, R.; Li, H.; Christoe, M. J.; Han, J.; Wang, Y.; Zhang, C.; Rahim, M. A.; Tang, J.; Yang, J.; Esrafilzadeh, D.; Jalili, R.; Allioux, F.-M.; O'Mullane, A. P.; Kalantar-Zadeh, K. *ACS Nano* **2020**, *14*, 14070–14079.
- (42) Wang, Y.; Guo, J.; Fang, Y.; Pang, G.; Wang, J.; Wang, X.; Jiao, C.; Chen, X.; Sun, K.; Hu, L. *Adv. Mater. Interfaces* **2021**, *8*, 2100954.
- (43) Chen, S.; Liu, J. *J. Phys. Chem. B* **2019**, *123*, 2439–2447.

□ Recommended by ACS

Flexible and Implantable Polyimide Aptamer-Field-Effect Transistor Biosensors

Chuanzhen Zhao, Anne M. Andrews, et al.

NOVEMBER 18, 2022

ACS SENSORS

READ ▶

Mineralization of Dandelion as an Enzyme-like Nanoelectrode for Ultrasensitive Monitoring of H₂O₂ at a Single-Cell Level

Xiaoxia Jian, Yan-Yan Song, et al.

AUGUST 12, 2022

ACS SUSTAINABLE CHEMISTRY & ENGINEERING

READ ▶

On the Move-Sensitive Fluorescent Aptassay on Board Catalytic Micromotors for the Determination of Interleukin-6 in Ultra-Low Serum Volumes for Neonatal Sepsis Diagnos...

José Gordón, Alberto Escarpa, et al.

OCTOBER 05, 2022

ACS SENSORS

READ ▶

Ultrasensitive Detection of MCF-7 Cells with a Carbon Nanotube-Based Optoelectronic-Pulse Sensor Framework

Sophia S. Y. Chan, Desmond K. Loke, et al.

MAY 26, 2022

ACS OMEGA

READ ▶

Get More Suggestions >